Journal of The Electrochemical
Society

Experimental Analysis of the Co-Electrolysis Operation under Pressurized Conditions with a 10 Layer SOC Stack

To cite this article: M. Riedel *et al* 2020 *J. Electrochem. Soc.* **167** 024504

Journal of The Electrochemical Society, 2020 **167** 024504

Experimental Analysis of the Co-Electrolysis Operation under Pressurized Conditions with a 10 Layer SOC Stack

M. Riedel,[1,z] M. P. Heddrich,[1] and K. A. Friedrich[1,2]

[1]German Aerospace Center (DLR), Institute for Engineering Thermodynamics, 70569 Stuttgart, Germany
[2]Institute of Building Energetics, Thermal Engineering and Energy Storage (IGTE), University of Stuttgart, 70569 Stuttgart, Germany

This study examines the performance of a solid oxide cell (SOC) stack during co-electrolysis of CO_2 and H_2O at elevated pressures up to 8 bar. Steady-state and dynamically recorded $U(i)$-curves were performed in order to evaluate the performance over a wide temperature range and to quantify the area specific resistance (*ASR*) at different pressure levels. Furthermore, the outlet gas composition at various current densities was analyzed and compared with the thermodynamic equilibrium. The open circuit voltage (*OCV*) was found to increase with higher pressure due to well known thermodynamic relations. An increase of the limiting current density at elevated pressure was not observed for the investigated stack with electrolyte supported cells. The *ASR* of the stack was found to decrease slightly with higher pressure. It revealed an increase of the cell resistance with lower H/C ratios in the feed at lower temperatures, whereas the performance of the co-electrolysis was very similar to steam electrolysis for temperatures above 820 °C. Within an impedance study for steam, co- and CO_2 electrolysis operation it was shown that pure CO_2 electrolysis exhibits a higher pressure sensitivity compared to pure steam or co-electrolysis due to significantly increased activation and diffusion resistances.

[DOI: 10.1149/1945-7111/ab6820]

Manuscript submitted October 2, 2019; revised manuscript received December 12, 2019. Published January 17, 2020.

List of symbols

Latin letters

U	Voltage, V
i	Current density, $A \cdot cm^{-2}$
ASR_{total}	Total area specific resistance, $\Omega \cdot cm^2$
ASR_{pol}	Area specific polarisation resistance, $\Omega \cdot cm^2$
ASR_{Ω}	Area specific ohmic resistance, $\Omega \cdot cm^2$
slpm	Standard liters per minute, $l \cdot min^{-1}$
RC	Reactant Conversion, %
p	Pressure, bar
R_{MF}	Resistance of the middle frequency process, $\Omega \cdot cm^2$
R_{LF}	Resistance of the low frequency process, $\Omega \cdot cm^2$
J_i	Area specific inlet gas flux with the unit of mol cm^{-2} s^{-1}
$x_{i,educt}$	Mole fraction of educt in the inlet gas, %
$x_{i,product}$	Mole fraction of product in the inlet gas, %
V	CSTR volume, m^3
A	geometric electrode area, m^2
f	Frequency, Hz
x_b	Mole fraction of product or educt in the bulk, %
D_{eff}	Effective diffusion coefficient, $m^2 \cdot s^{-1}$

The goals set by the European Union for the near future until 2050 foresee a stringent reduction of the proportion of fossil fuels in all sectors, in particular also in power, transport and industry.[1] Moreover, the constant increase of electric power from renewables will enable new uses apart from electricity if the technologies for conversion are flexible, efficient and economical.[2–4] Especially cross-sectoral use with a storage function in the area of combined heat and power, transport and chemical industry will be of essential importance. Producing chemicals from steam and CO_2 with solid oxide electrolysis cells (SOECs) as energy converters could become a key technology for expanding the energy transition beyond the electricity sector.[5,6] Due to the high operating temperature (>700 °C), SOECs offer significant benefits like high thermodynamic efficiency, fast kinetics and reduced electrochemical losses with steam electrolysis. Moreover it is possible to conduct co-electrolysis operation to convert H_2O and CO_2 simultaneously into synthesis gas ($H_2 + CO$). This syngas can be used as feedstock for the production of base chemicals or synthetic fuels in downstream processes. Fischer–Tropsch or methanol synthesis reactors are typically operated at elevated pressures in the range of 10 to 60 bar to achieve high conversion or high yield.[7–9] Furthermore storage and transportation of gaseous products also require pressurization of the products. Combining a SOEC stack and the catalytical downstream reactor in a pressurized system could therefore be highly beneficial since additional compression work could be significantly reduced or omitted.[10] Furthermore, previous studies have shown that with increasing the pressure, the total area specific resistance (ASR_{total}) decreases significantly with fuel electrode supported cells.[11–15]

During co-electrolysis operation H_2O and CO_2 reduction occur at the fuel electrode and require energy supply due to the endothermic properties of the reactions shown in Eqs. 1 and 2. Additionally, both reactions are related via the endothermic reverse-watergas-shift (rWGS) reaction shown in Eq. 3:

$$H_2O \rightarrow H_2 + \tfrac{1}{2}O_2 \quad \Delta H_r(860\,^{\circ}C) = +249\ kJ \cdot mol^{-1} \qquad [1]$$

$$CO_2 \rightarrow CO + \tfrac{1}{2}O_2\ \Delta H_r(860\,^{\circ}C) = +283\ kJ \cdot mol^{-1} \qquad [2]$$

$$H_2 + CO_2 \rightarrow H_2O + CO\ \Delta H_r(860\,^{\circ}C) = +34\ kJ \cdot mol^{-1} \qquad [3]$$

The high temperature electrolysis mode requires the enthalpy of formation for the reactions to be provided as electrical and thermal energy. Figure 1 shows the energy demand for the reactions shown in Eqs. 1 and 2 over temperature at standard pressure.

The total energy demand (ΔH) slightly increases for H_2O reduction and is nearly constant for CO_2 reduction respectively whereas for both reduction reactions the electrical energy demand (ΔG) strongly decreases and the thermal energy demand ($T \cdot \Delta S$) increases with temperature accordingly. As depicted in Fig. 1 the CO_2 reduction generally requires a higher amount of thermal (and total) energy supply whereas the electrical energy demand is fairly equal with water reduction at temperatures >750 °C. In literature the co-electrolysis operation is sometimes stated to solely take place via electrochemical steam reduction and CO is purely produced by rWGS reaction.[16,17] The additional thermal energy demand of the rWGS leads to lower stack temperatures and increased

---

[z]E-mail: Marc.Riedel@dlr.de

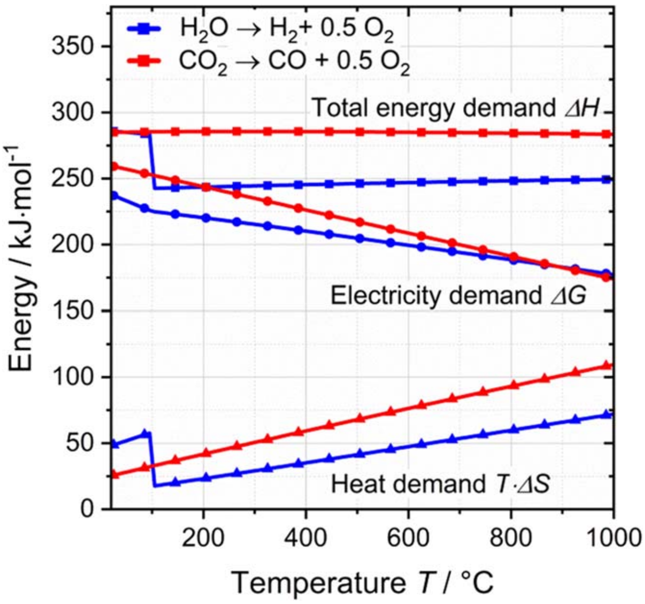

Figure 1. Energy demand of the H_2O and CO_2 reduction reactions depicting the total energy demand (reaction enthalpy ΔH, squares), the electricity demand (Gibbs free reaction energy ΔG, points) and the heat demand ($T \cdot \Delta S$, triangles).

overpotentials. Furthermore, SOECs operated in pure CO_2 electrolysis mode reveal a significantly higher thermoneutral voltage than steam electrolysis operation due to the higher enthalpy of the related reduction reaction.

Test Setup

In this study a commercially available stack with 10 electrolyte supported cells was used. Each cell consists of a Ni-CGO fuel electrode, a 3YSZ electrolyte and a LSCF air electrode. Additionally, CGO barrier layers are implemented between the fuel electrode/electrolyte and the air electrode/electrolyte respectively. Since the stack has an open oxygen electrode design, it is housed in a specially designed gas tight steel box. For measuring the temperatures inside the stack during operation, five thermocouples are placed directly on the air electrodes. One thermocouple is placed on layer one and ten respectively. The three remaining thermocouples are placed at quarter, half and three-fourths of the length of the middle cell of the stack. Further details about the stack and the implementation into the test setup are already published and can be found elsewhere.[18]

The experimental test setup at DLR offers the opportunity to characterize short stacks in SOEC as well as in SOFC mode in an absolute pressure range between 1.4 and 8 bar. Figure 2 shows the schematic of the test setup which mainly consists of the media supply (A), the pressurized vessel with an integrated oven (C) and the pressure control combined with two equalizing tanks for the anode and cathode streams (D). A stable and low pulsation steam supply is assured by an evaporator without the use of carrier gas (B). Ultrapure water for evaporation is stored in a water tank with an integrated UV-lamp and is continuously circulated through a self-constructed water purification system with fine filters and a desalination unit in order to prevent any contaminants entering the test rig and/or lead to enhanced degradation of the investigated stacks. Except the steam, all feed gases are supplied via mass flow controllers at the gas supply panel. Before entering the pressure vessel, the feed gases are heated to 300 °C via an electric heater and are mixed with the required steam mass flow in order to prevent condensation and thus caused pressure drops and instable cell voltages. The mixture is led through the vessel wall and is further heated via an electric preheater to the furnace temperature before entering the stack. However, the carbon containing gases (CO, CO_2 or CH_4) are led directly via a stub to the furnace compartment in order to prevent solid carbon deposition in the preheater due to the possible lower heating rates. The carbon containing gases are mixed with the remaining gases of the preheater upstream of the stack.

In order to maintain very small differential pressures between fuel side, air side and the surrounding furnace atmosphere (<5 mbar), a highly sensitive pressure control system is implemented in the test rig. Differential pressure sensors at the outlet pipes are constantly surveilling the pressure differences between the pressure vessel and the fuel outlet stream and between the fuel side and the air side. To enable a precise pressure control, the gas volumes of the anode and cathode side have to match the vessel volume and are therefore balanced by two equalizing tanks (D, 500 l each). The pressures in the equalizing tanks are controlled by pneumatic valves, which let specific volumes stream into the off-gas burner to match the exact pressure difference between the gas compartments. The fuel side is generally operated at slightly higher pressure in order to prevent gas transition towards the air electrode in case of cell leakages.

The pipe connecting the fuel outlet of the stack and the equalizing tank of the fuel side is constantly heated to 250 °C to prevent condensation of the containing steam content and thus an instable voltage of the upstream-located stack. In order to prevent solid carbon deposition within the outlet pipe of the test setup during co- and CO_2-electrolysis studies, a second water evaporator is installed (B). Generally, solid carbon can deposit during the chilling of the produced hot CO or syngas in the outlet pipes and could clog the whole system with a likely associated damage to the stack. The risk of carbon deposition especially takes place in a temperature range between 500 °C–700 °C and becomes more severe with higher operating pressures. Therefore, the second evaporator injects additional steam directly behind the stack outlet and increases the partial pressure of H_2O in the fuel outlet pipe. Combined with a rather quick cross of the risky temperature window to 250 °C, no carbon deposition occurred during the presented studies of this publication. Due to that configuration, detailed investigations of risky operation conditions can be made without endangering the test facility or the stack. Figure 3 shows a theoretical consideration for the amount of steam need to be injected into the fuel outlet pipe to prevent solid carbon deposition based on thermodynamic equilibrium. $\dot{m}_{H2O}^{add}$ represents the mass flow of steam to be injected into the outlet pipe and $\dot{m}_{react}$ is the mass flow of gas which is supplied to the stack at the media inlet. The gas inlet composition and the reactant conversion (*RC*) are in accordance to the experimental parameters used in this study where a considerable risk of solid carbon formation due to the low H/C ratio of 2.44 (inlet gas composition 45% H_2O, 45% CO_2 and 10% H_2) exists. 1.4 bar is the lowest, 8 bar the highest possible operating pressure of the described test rig at DLR. Furthermore, the theoretically needed steam injection to prevent carbon deposition at an operating pressure of 30 bar is shown in the graph. This pressure level represents the operation of a co-electrolysis system with a directly coupled downstream process e. g. Fischer–Tropsch where much higher pressures are needed.

Due to slower reaction kinetics at lower temperatures and the limitation of catalytic reaction sites in the steel pipe, the values given in Fig. 3 can be considered to be maximum values for a safe operation of a pressurized test setup. Experimental investigations showed that the injection of additional steam into the outlet pipe of the test rig does not affect the *OCV* or performance of the stack in all investigated cases.

In order to constantly monitor the outlet gas composition of the stack, a gas analyzing system is connected to the test rig (Fig. 1e). During the experiments a continuous gas flow of 1 slpm is taken from the fuel outlet pipe and sent to a Rosemount X-Stream analyzer with sensors for H_2, CO, CO_2 and CH_4. Due to the optical measuring principle of this analyzer the steam of the gas mixture is removed via a compressor chiller operated at 3 °C. All gases can be analyzed in a range of 0%–100% with an accuracy of $\leqslant \pm 1\%$.

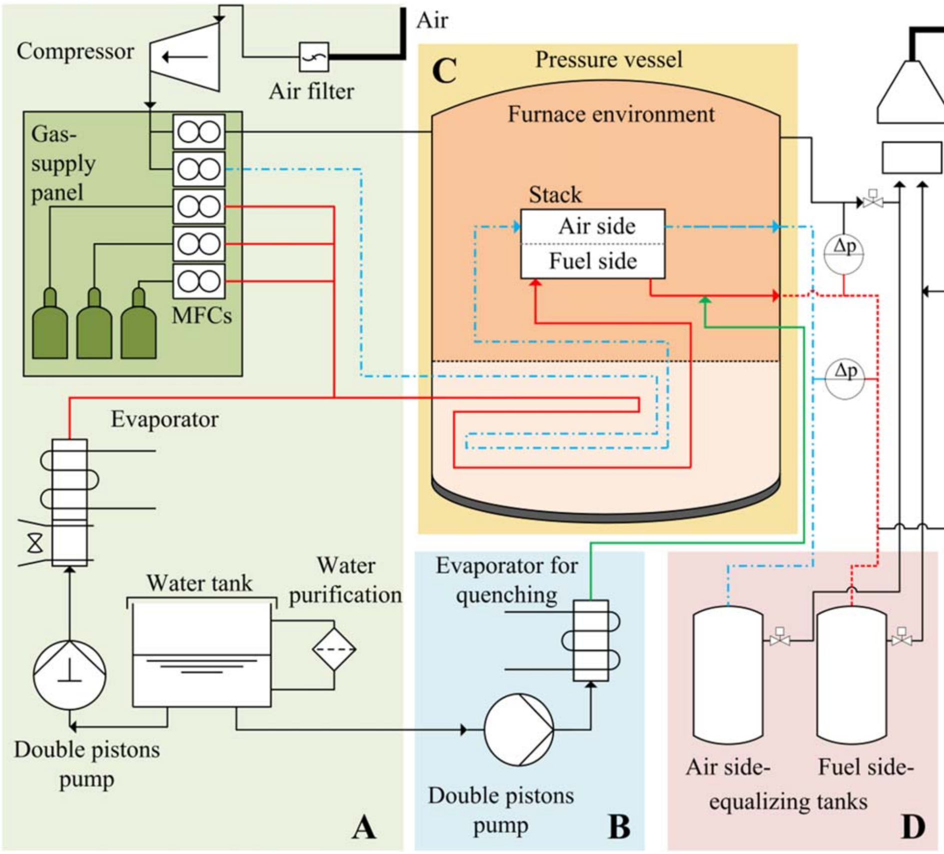

Figure 2. Schematic of the experimental test setup for pressurized SOC stack investigations at DLR.

Experimental Methodology

In this study two inlet gas compositions were used with an H/C ratio of 2.44 (45% H_2O/45% CO_2/10% H_2) and 4.67 (60% H_2O/30% CO_2/10% H_2). Steady-state as well as dynamically recorded current-voltage curves were performed for characterizing the stacks under pressurized operation in co-electrolysis mode. For steady-state U(i)-curves, current density was increased stepwise by 78.24 mA·cm^{-2}(≙ 10 A steps). The gas flows for each composition were adjusted at every current density point for a constant reactant conversion (RC) of 70% at the cells. The RC is always defined according to the overall inlet mass flow of convertible reactants, i.e. the overall amount of H_2O and CO_2 during co-electrolysis operation that can be converted to H_2 and CO (and not further to C). A constant flux of air was supplied to the stack on the anode side. Reaching stationary conditions in the stack took at least 90 min depending on the operating point. The outlet gas composition was constantly monitored during all experiments. Due to this method it is possible to record a U(i)-characteristic with a current density dependent temperature and gas composition profile at a constant reactant conversion rate.

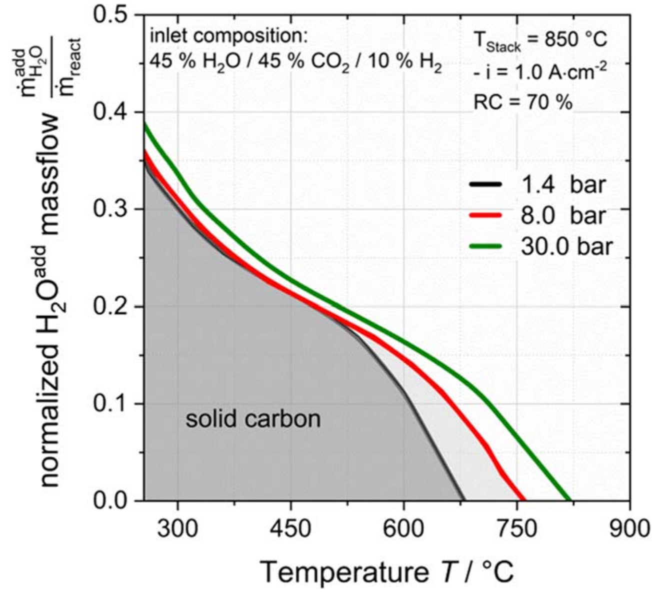

Figure 3. Ratio between mass flow of steam to be injected ($\dot{m}^{add}_{H2O}$) and the inlet mass flow of gas supplied to the 10 layer stack ($\dot{m}_{react}$) in order to prevent carbon deposition during chilling in the outlet pipe. Calculations are based on thermodynamic equilibrium for an inlet composition of 45% H_2O, 45% CO_2 and 10% H_2 at a stack temperature of 850 °C and a conversion rate of 70% at a current density of -1.0 A·cm^{-2}.

In contrast, dynamically recorded U(i)-curves were performed with a fast increase of current density of 1.96·10^{-3} A·cm^{-2}·s^{-1} (≙20 A min^{-1}). The gas flows were defined for a reactant conversion of 70% at -0.47 A·cm^{-2}. 10 slpm air was supplied to the anode side of the stack. Due to the fast current ramp a quasi-isothermally recorded $U(i)$-curve with a very small temperature change over the complete range of current density could be performed.

Electrochemical impedance analysis was performed galvanostatically with a Zahner Zennium at -0.20 A·cm^{-2} with an AC amplitude of 380 mA. The frequency range for impedance spectroscopy was defined to be in the range of 20 kHz to 50 mHz with single sine wave impedance. The recorded spectra were analyzed with the commercial software THALES.

The stack was operated over approximately 700 hours for the characterizations of the steam, co-, and CO_2 electrolysis shown in this study. A significant degradation during that operating time was not observed.

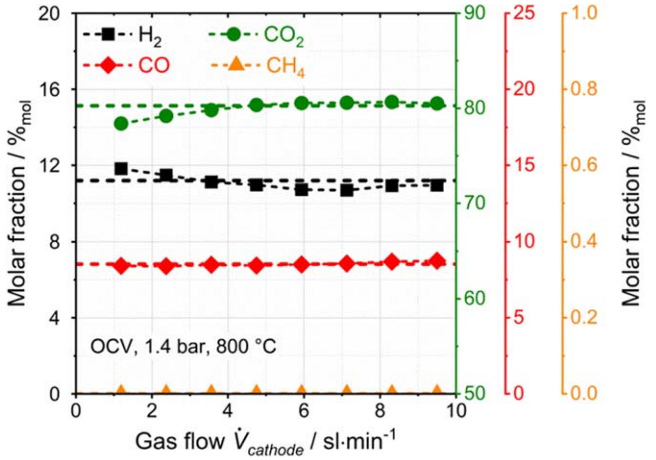

Figure 4. Comparison between thermodynamic equilibrium and the measured outlet gas composition of the stack operated with an inlet composition of 45/45/10 ($H_2O/CO_2/H_2$), at 1.4 bar and 800 °C over the full range of volume flows for the steady-state *U*(*i*)-curves shown in Fig. 5.

Results and Discussion

Steady state U(i)-characteristics and gas analysis.—Before starting the experimental investigations, the stack was operated in non-loaded conditions with a 50/50 mixture of hydrogen and nitrogen at 800 °C. The temperatures measured inside the stack were equal to furnace temperature and the stack voltage was above 12.5 V. Hence, leakages were considered to be negligible.

To exemplify the accuracy of the gas analyzing system, Fig. 4 shows the recorded outlet gas composition during stack measurements at *OCV* conditions, 1.4 bar, a stack temperature of 800 °C and an inlet gas composition of 45/45/10 ($H_2O/CO_2/H_2$). At *OCV* condition and at a constant furnace temperature, an effect of the occurring endothermic rWGS reaction cannot be noticed since the content of reducing gas (H_2, CO) in the used feed composition is low and the extent of reaction is therefore limited. The outlet gas composition was analyzed over the full range of inlet volume flows according to the steady-state U(i)-curves with 70% reactant conversion presented in Fig. 5. The maximum flow corresponds to a current density of 0.63 A·cm^{-2}. Note that H_2O is completely removed out of the outlet gas composition by the gas analyzing system due to its measuring principle. The straight lines represent the thermodynamic equilibrium of the gases H_2, CO, CO_2 and CH_4 respecting a H_2O-free gas composition. Thermodynamic equilibrium was calculated with the CEA tool (Chemical Equilibrium with Applications) and the included gas properties published by the National Aeronautics and Space Administration (NASA).[19]

The maximum deviation between the thermodynamic equilibrium and the experimentally recorded measurement points can be found at small gas flows supplied to the stack. The maximum deviation of 1.9%-points (CO_2) can likely be attributed to the increasing inaccuracy of the mass flow controllers at small gas flows. Note that the impact of the inaccuracy on the *OCV* is marginal due to the present reducing gas content (H_2, CO) of more than 10%. Generally, the outlet gas composition is in good accordance to the calculated thermodynamic equilibrium over the full range of inlet volume flows. Firstly, this indicates the precise supply of the feed gases and the analytical system to work accurately over a wide range

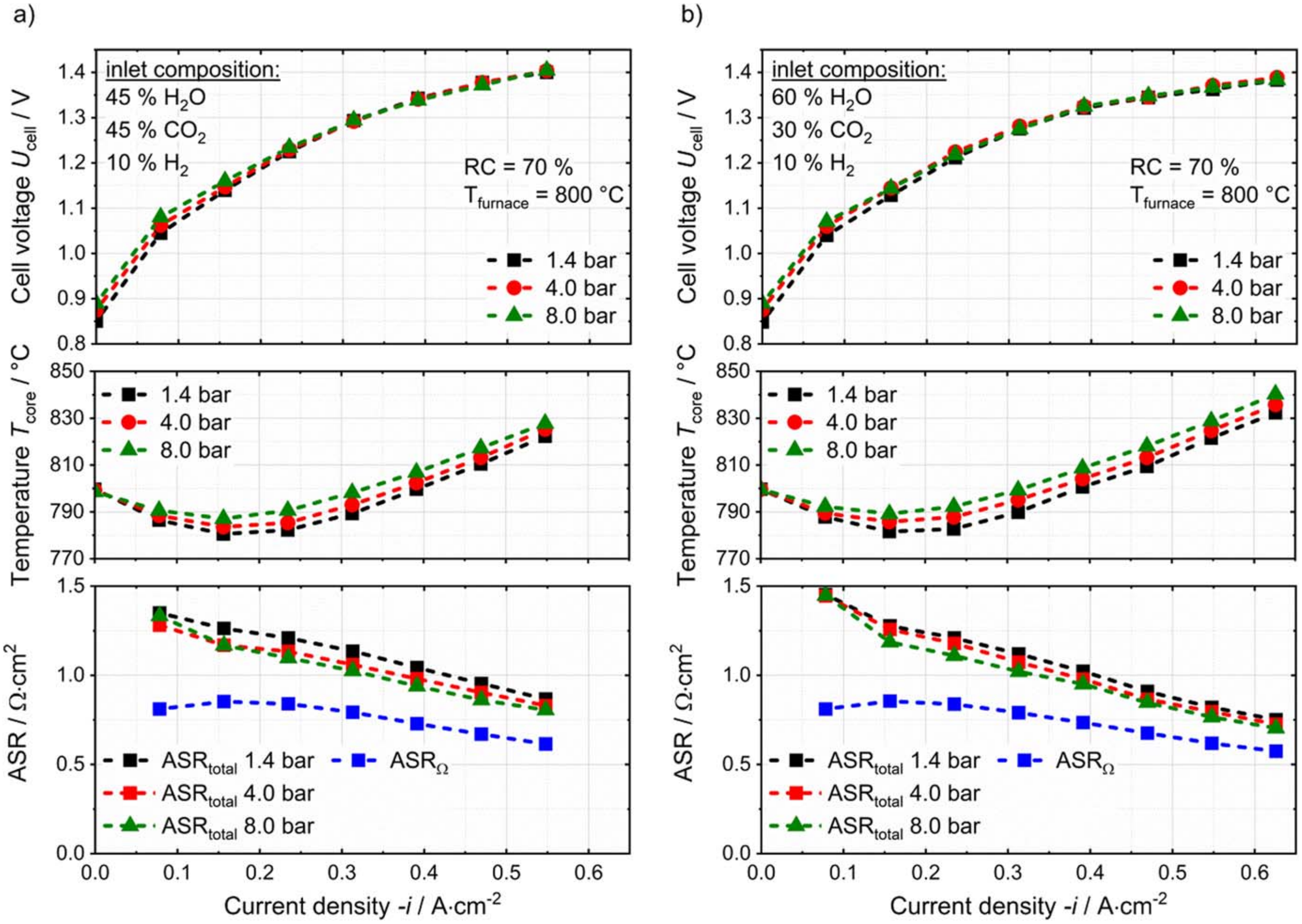

Figure 5. Steady-state U(i)-curves recorded at 1.4, 4 and 8 bar at a furnace termperature of 800 °C. Inlet gas composition is (a) 45/45/10 ($H_2O/CO_2/H_2$) and (b) 60/30/10 ($H_2O/CO_2/H_2$) with a reactant conversion of 70**%** at every measuring point.

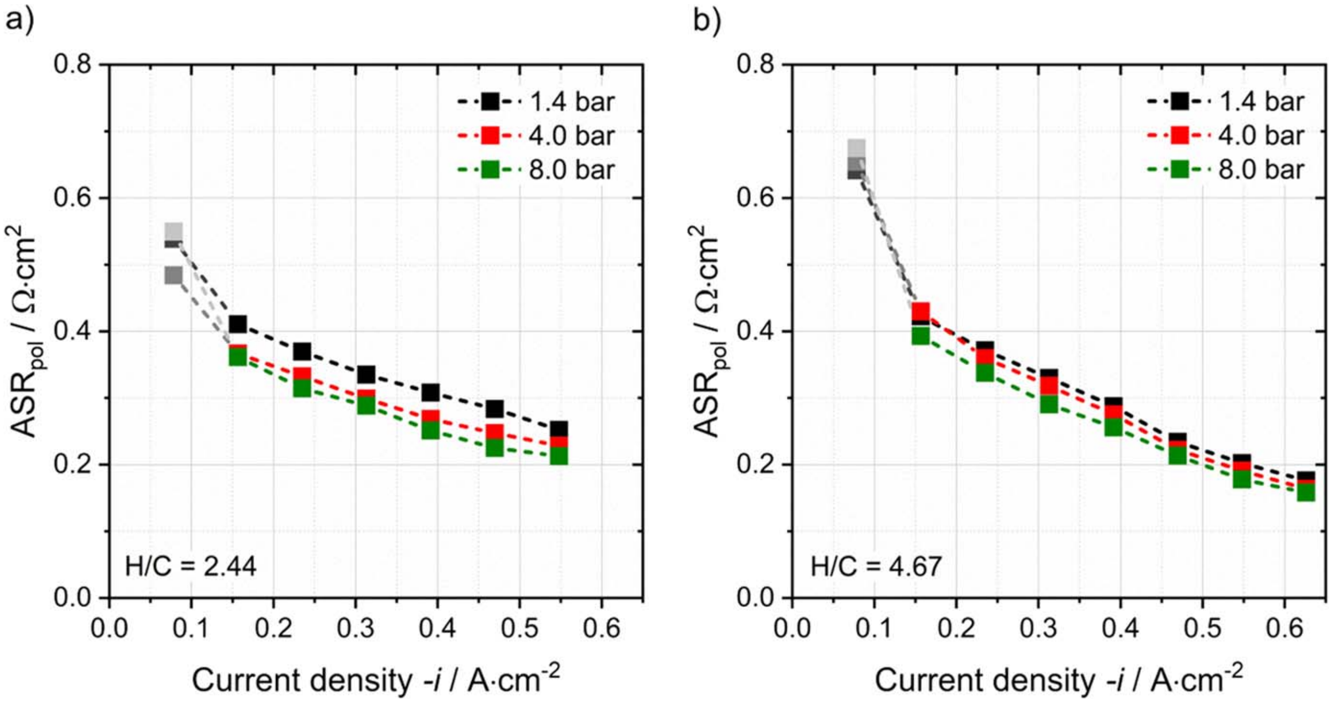

Figure 6. Polarization resistance for the steady-state $U(i)$-curves recorded at 1.4, 4 and 8 bar at a furnace termperature of 800 °C.

of operation. Secondly, it shows that the chemical reactions are fast and the catalytic surface is sufficiently active and available to equilibrate the inlet gases rapidly within the cells via the reverse water-gas shift reaction (rWGS).

Figure 5 shows steady-state $U(i)$-curves with the inlet compositions 45/45/10 and 60/30/10 ($H_2O/CO_2/H_2$) for 1.4, 4 and 8 bar and a furnace temperature of 800 °C. The inlet gas compositions correspond to an H/C ratio of 2.44 and 4.67 respectively. The cell voltage of the middle cell, the core temperature of the stack and the calculated total ASR (ASR_{total}) are plotted against the current density. Furthermore the ohmic ASR (ASR_{Ω}) is plotted based on the core temperature of the stack for the measurements at 1.4 bar. An equation for the temperature-dependency of the ohmic resistance of the studied stack was already published by the authors and can be found in.[18]

For calculating the ASR_{total} the conversion is considered to be linear over the cell length. The theoretical voltage at every measuring point is hence calculated with the equilibrated averaged gas composition between inlet and outlet of the stack and the actual measured stack temperature. The justification of that method for calculating the ideal voltage is published elsewhere.[20] The ASR_{total} was subsequently calculated by dividing the difference between theoretical and measured voltage by the current density.

As can be seen, both experiments on co-electrolysis show similar performance although the H/C ratio is different by a factor of almost 2. As expected, the open circuit voltages were found to increase with increasing operating pressure. In the range of low current densities, the influence of thermodynamics on the stack and cell performance is more significant than the influence of electrochemical reaction kinetics. The core temperatures of the stack decrease at low current densities due to the endothermic reduction reaction of H_2O (and CO_2), the endothermic rWGS reaction and the comparably low overvoltages at low currents. With higher current densities the stack temperature increases due to the higher heat generation (or higher losses).

By increasing the current density, the cell voltages are found to converge, particularly the $U(i)$-curves recorded at 4 and 8 bar show a decreased slope in both cases. This could be attributed to the measured stack temperature which increased with higher pressures due to the occurring internal methanation reaction. The higher temperature lowers the cell voltage due to the reduced cell resistance which may explain the convergence with higher pressures. Furthermore, at elevated pressure internal cell resistances are known to decrease due to superior mass transport and decreased diffusion overpotentials.[21–24] Hence, the impact of pressurization on cell performance becomes more significant with higher current densities. To exemplify, in Fig. 5a the maximum spread of the characteristic stack temperature between 1.4 and 8 bar is 8.9 K at a current density value of $-0.39\ \mathrm{A \cdot cm^{-2}}$. According to the relation published in[18] this temperature spread leads to a deviation of the ohmic resistance of 0.055 $\Omega \cdot \mathrm{cm}^2$. At this current density point the deviation of the calculated ASR_{total} between 1.4 and 8 bar is 0.110 $\Omega \cdot \mathrm{cm}^2$ and thus two times higher than the ohmic resistance spread. At the highest investigated current density of $-0.54\ \mathrm{A \cdot cm^{-2}}$, the temperature deviation between 1.4 and 8 bar is 5.5 K, which corresponds to 0.023 $\Omega \cdot \mathrm{cm}^2$ in ohmic resistance. The ASR deviation at this measuring point is 0.062 $\Omega \cdot \mathrm{cm}^2$, thus almost three times higher than the ohmic resistance deviation.

Comparing both experiments with different inlet compositions, Fig. 5a with the higher content of carbonaceous gas in the feed shows a slightly increased cell voltage and subsequently a decreased maximum achievable current density. The performance loss indicates the contribution of an increased diffusion and activation overpotential with increasing CO_2 content in the feed gas. However, the measured stack temperatures show almost same values in both experiments.

The bottom charts in Fig. 5 show the calculated ASR_{total} for each recorded current density step based on the measured characteristic stack temperature. The ASR_{Ω} represents the specific ohmic resistance for the measured temperatures at 1.4 bar and follows the temperature profile shown in the graph above. Due to the fact that for ESC stacks the overall cell resistance is dominated by the ohmic part, the ASR_{total} was expected to follow the shape of the ASR_{Ω} curve. Though, at low current densities the ASR_{total} shows comparably high values for both co-electrolysis experiments at every operating pressure. Most likely this behavior results from the inaccuracy of the mass flow controllers of the test rig at little gas flows as shown in Fig. 4 where a slightly increased molar fraction of H_2 and a simultaneously decreased CO_2 fraction were found at the outlet. The inaccuracy leads to slightly higher measured voltages and hence to a higher calculated ASR_{total}. With increasing current density and stack temperature, Fig. 5 indicates that the polarization resistance, derived from the difference between ASR_{total} and ASR_{Ω} decrease with current density. In Fig. 6 the polarization resistances are plotted against current density for each pressure. Note, the points related to a current density of 0.08 $A\cdot cm^{-2}$ are plotted in grey due to the inaccuracy of the mass flow controllers according to Fig. 4 and will not be part of further analysis.

Comparing both experiments, the polarization resistances show higher values for the lower H/C ratio which is congruent with the findings of the higher ASR_{total} with the higher CO_2 content in the feed gas shown in Fig. 5. With increasing current density, the polarization resistances are found to decrease due to the higher stack temperature and the consequently faster reaction kinetics. Furthermore the activation and diffusion resistances are known to decrease with elevated pressure. However, the pressure dependency was already found to be marginal due to the thin electrodes and the comparably high ohmic resistance of the ESCs used in the studied stack. Hence, the decrease of the polarization resistances at higher pressures is induced by two effects: the faster reaction kinetics due to higher temperature and the decrease of the activation and diffusion resistances due to the elevated operating pressure.

During the co-electrolysis experiments, the outlet gas composition at every stationary current density step was recorded. Figure 7 shows the measured values of H_2, CO, CO_2 and CH_4 for 1.4 bar (squares), 4 bar (dots), 8 bar (triangles) and the thermodynamic equilibrium based on the measured stack temperature (dashed lines). As described above, the steam content is removed out of the mixture before the analyzer due to its optical measurement principle.

The measured concentrations for the outlet gases are in good accordance with the calculated thermodynamic equilibrium over the full range of current density. As can be seen, in both experiments the major deviation between theoretical and experimentally recorded values can be found at low current densities, especially for H_2 and CO_2. As mentioned above, this is likely due to an inaccurate dosage of the mass flow controllers of the test rig at little gas flows. The experimental results of the gas analysis indicate that the rWGS and the methanation reactions are fast and shift the gas mixture into equilibrium within the stack even at high flow rates and a RC of 70%.

For high methanation extent of reaction, high pressures, high H_2/CO ratios and low temperatures are favorable. During the experiments a methane content of almost 5% was measured at 8 bar and 790 °C for the inlet composition of 60/30/10 ($H_2O/CO_2/H_2$) with the H_2/CO ratio of 2.5 after 70% conversion. With higher current densities the methane content was found to decrease due to the increased stack temperature and thus a decreasing H_2/CO ratio. Within the conducted experiments, the H_2/CO ratio at the stack outlet is in a range of 1.18-1.27 for the inlet composition of 45/45/10 and between 2.31-2.48 for the 60/30/10 composition.

The measured temperature distribution within the stack during the steady-state co-electrolysis operation with the 45/45/10 mixture at 1.4 and 8 bar is shown in Fig. 8. The nomenclature of the temperatures $T_{i,j}$ in the legend indicate the position of the thermocouple in the stack. i is the specific layer and j the position along the flow direction of the active cell area where the thermocouple is located.

The recorded temperatures show a maximum deviation of 5.9 K at 1.4 bar and 6.3 K at 8 bar in the endothermic operating mode. In the exothermic mode it is 6.1 K and 12.9 K respectively. As expected, the surrounding furnace environment shows the most significant thermal influence on both outer layers of the stack ($T_{L1,1/2}$ and $T_{L10,1/2}$) at both pressures. During endothermic operation both layers have the highest and in exothermic operation the lowest temperature. The temperatures measured along the flow direction of layer 5 show a maximum deviation of 3.9 K at 1.4 bar and 8.7 K at 8 bar, whereas the thermocouple close to the inlet ($T_{L5,1/4}$) always recorded the lowest and the thermocouple close to the outlet ($T_{L5,3/4}$) the highest values. The temperature profile along the height of the stack contributes to the inequality of the cell voltages shown in Fig. 8b. As can be seen, at maximum current density the cell voltage of layer 10 show the maximum deviation of 45 mV.

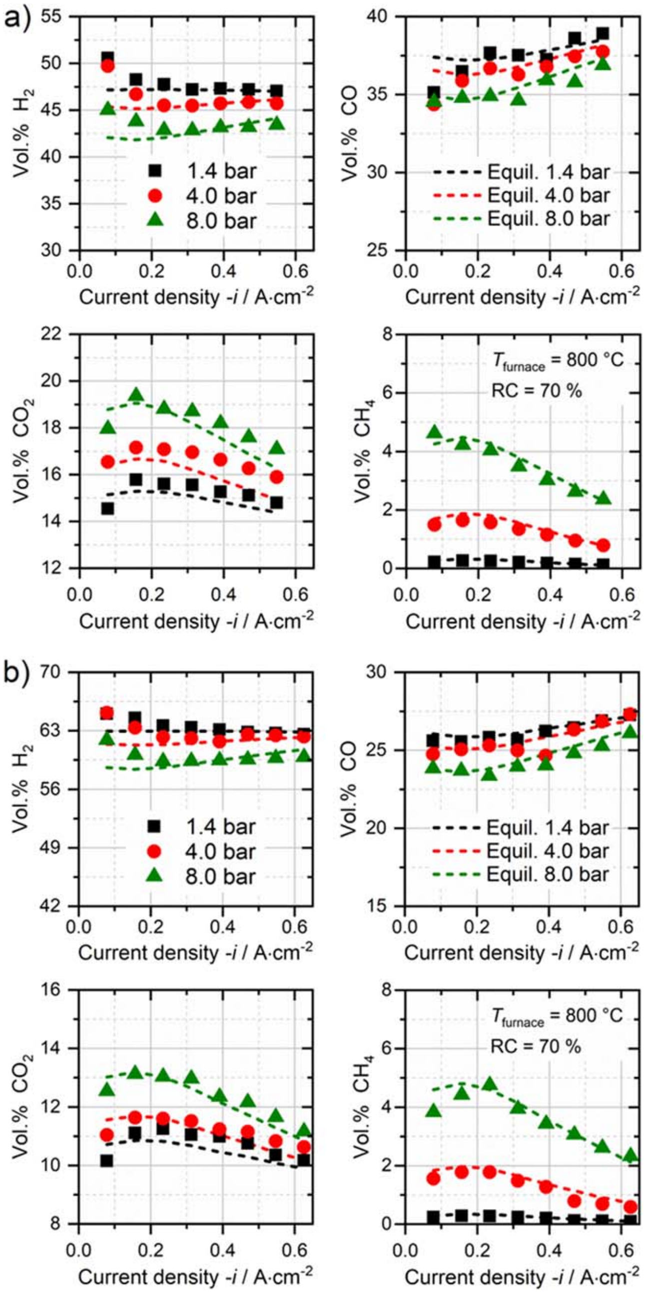

Figure 7. Gas analysis of the stack outlet composition during the steady state co-electrolysis experiments for an inlet composition of (a) 45/45/10 ($H_2O/CO_2/H_2$) and (b) 60/30/10 ($H_2O/CO_2/H_2$). The reactant conversion is 70%.

Dynamically recorded U(i)-characteristics.—The aim of the dynamically recorded $U(i)$-curves is the quasi-isothermal characterization with only a small temperature deviation within the stack. This ensures determining the performance at a certain stack temperature. Figure 9 shows a comparison between co- and pure steam electrolysis at 800 °C and 850 °C with a reactant conversion of 70% at −0.47 $A\cdot cm^{-2}$. In both cases, the voltage shows an nearly linear behavior up to the maximum current density with a slightly decreased slope of the $U(i)$-curves recorded at elevated pressure.

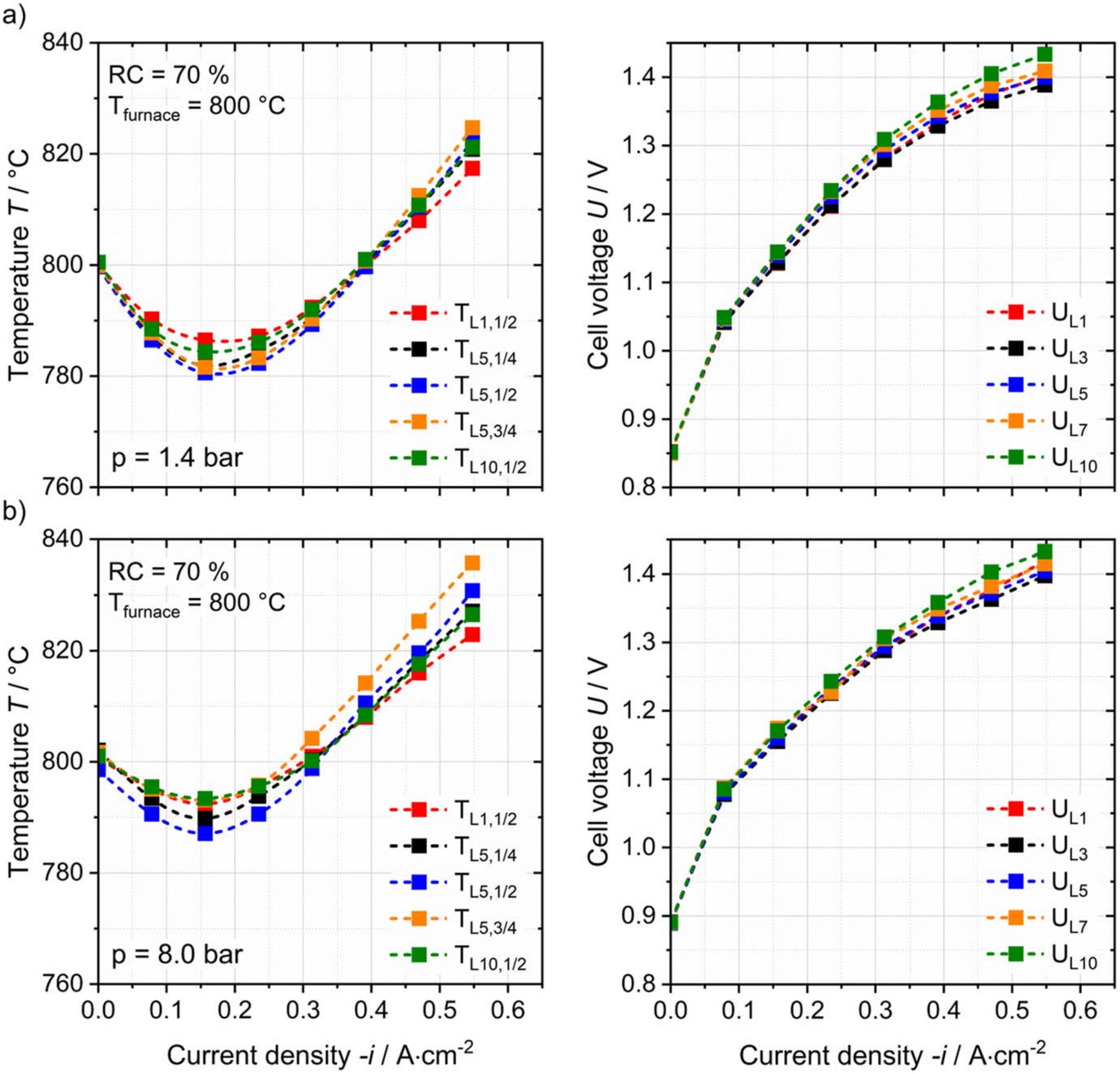

Figure 8. Measured temperatures and cell voltages of the stack during the steady-state co-electrolysis experiment at 1.4 and 8 bar respectively and an H/C ratio of 2.44 in the feed gas (45/45/10 mixture).

However, an overall positive pressure effect on the achievable current density could not be observed for the ESC stack at the studied steam- or co-electrolysis conditions.

Determination of the area specific resistance during co-electrolysis operation.—In order to determine the ASR values, the theoretical Nernst voltage is calculated based on the actual current dependent gas composition and the measured characteristic stack temperature for every measuring point due to the increasing conversion rate over the recorded current density. Note, for co-electrolysis operation the averaged gas composition between the inlet and outlet of the stack is equilibrated before calculating the theoretical voltage. The ASR values shown in the graphs are averaged values in the range of $0.08\,\mathrm{A \cdot cm^{-2}}$ to the maximum achieved current density of the experiment. As depicted in the graphs, the increase of 50 K furnace temperature leads to a decrease of the ASR by almost 30%.

Due to increased temperature deviations over the range of current density, the recorded $U(i)$-curves in co-electrolysis mode show slightly higher voltages and ASR values compared to pure steam electrolysis at both furnace temperatures. In co-electrolysis operation the measured temperature deviation is more significant at lower pressures due to the occurring endothermic rWGS reaction and less extent of exothermic methanation. At elevated pressure the voltage increases due to thermodynamics influence and the exothermal methanation reaction becomes more prominent. Hence, increasing heat production at elevated pressure contributes to counterbalance the characteristic of the pure endothermal electrolysis- and rWGS reactions and lead to decreased overvoltages. The described temperature behavior at higher pressures can also be observed for pure steam electrolysis. However the lower temperature deviation at higher pressure is solely caused by the thermodynamically driven higher voltages in that operating mode.

The following Table I shows the temperature deviations for the recorded $U(i)$-curves:

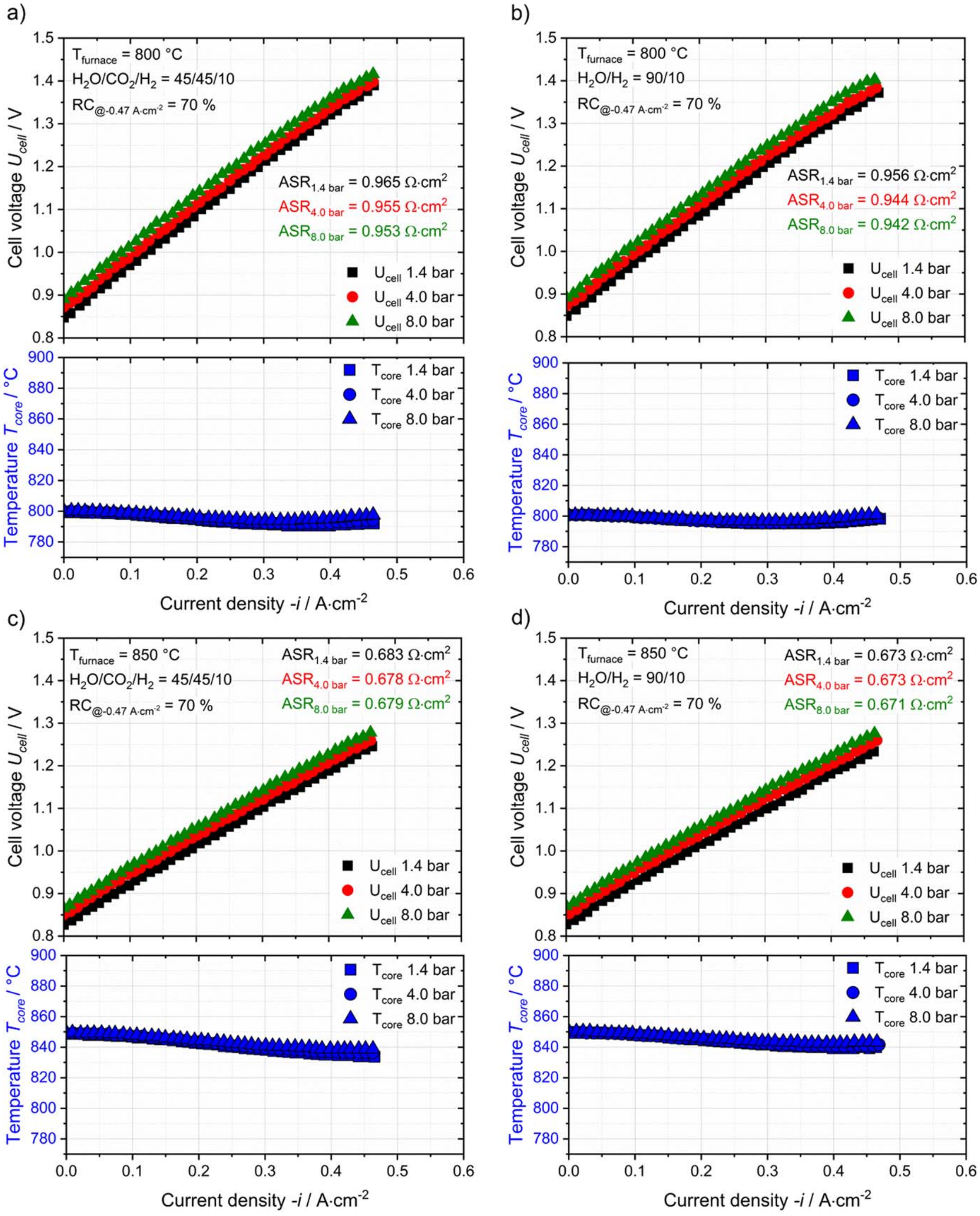

Figure 9. Dynamically recorded $U(i)$-curves at three different operating pressures a conversion rate of 70% at −0.47 A·cm^{-2} and 800 °C and 850 °C furnace temperature. (a) and (c) show the results for co-electrolysis, (b) and (d) for pure steam electrolysis operation.

The temperature deviation during co-electrolysis operation at 800 °C furnace temperature and 1.4 bar was found to be 8.7 K over the complete range of current density. The ASR_{total} was calculated to be 0.965 Ω·cm^2 accordingly. In pure steam electrolysis operation the ASR_{total} was calculated to be 0.950 Ω·cm^2 and a temperature deviation of 5.5 K was observed. Hence, the difference of the

Table I. Temperature deviations between furnace and the measured characteristic stack temperature over the complete current density range during dynamically recorded *U*(*i*)-curves in steam- and co-electrolysis operation.

Furnace temperature/°C	Pressure/bara	Temperature deviation in Co-electrolysis 45/45/10 in K	Temperature deviation in H_2O-electrolysis 90/10 in K
800	1.4	8.7	5.5
800	4.0	8.0	5.2
800	8.0	6.3	4.2
850	1.4	14.9	10.0
850	4.0	12.9	9.0
850	8.0	10.8	7.6

characteristic stack temperature between steam and co-electrolysis operation is about 3.2 K ($\Delta ASR = 0.015\ \Omega\cdot\text{cm}^2$) at this pressure. The lower temperature during co-electrolysis operation leads to an increased ohmic resistance of about 0.017 $\Omega\cdot\text{cm}^2$.[18] At 8 bar the ΔASR_{total} was found to be 0.012 $\Omega\cdot\text{cm}^2$ with a ΔT of about 2 K. This leads to an increase of the ohmic resistance of 0.013 $\Omega\cdot\text{cm}^2$. Therefore it can be concluded that the performance of the stack within the studied dynamical conditions in pure steam- and in co-electrolysis is highly similar and mainly influenced by the stack temperature.

Out of dynamically recorded and steady state measurements for steam- and co-electrolysis operation, detailed characteristics of the ASR_{total} could be obtained for the studied ESC stack. Figs 10a–10c shows the ASR_{total} and the characteristic ASR_{Ω} over a wide temperature range for the inlet gas compositions of 45/45/10, 60/30/10 ($H_2O/CO_2/H_2$) and 90/10 (H_2O/H_2). The *ASR* values were fitted to the exponential expression $ASR_{total} = y_0 + A\cdot\exp(B\cdot T)$ and are furthermore plotted for all studied gas compositions in Fig. 10d.

During steam electrolysis operation the ASR_{total} follows the characteristic of the ohmic resistance with an additional and temperature dependent resistance. This additional part indicated by the difference between ohmic and overall resistance can be attributed to the polarization overvoltage. It accounts for approximately 20% of the overall resistance in steam electrolysis over a wide temperature range of the ESC. In case of co-electrolysis operation the polarization resistance shows a higher temperature dependency. At low temperatures the ASR_{total} shows a higher proportion of the polarization resistance while at high temperatures (>820 °C) a significant difference between steam- and co-electrolysis cannot be observed. Thus the increasing partial pressure of CO_2 has a worsening influence on the cell and stack performance during co-electrolysis especially at lower temperatures. This could be related to the decreased partial pressure of steam at the TPB and thus the increased activation and concentration overpotentials. This would imply CO to be solely produced by the rWGS reaction. However it is very likely that for some extent CO_2 is reduced electrochemically which leads to higher overpotentials due to a higher required activation energy of the reduction process at the TPB and a higher diffusion overpotential due to its comparably larger molecular size and molecular mass.[25–27] Furthermore, the effective diffusion coefficient is proportional to the operating temperature. Both can lead to a higher diffusion overpotential at lower temperatures and thus an increased concentration overpotential.[21] Since at higher temperatures the influence of reaction kinetics is less prominent, the ASR_{total} of the co-electrolysis operation converges towards the ASR_{total} of steam electrolysis operation.

Impedance analysis during steam, co-, and CO_2 electrolysis operation.—EIS was performed in order to investigate in more detail the pressure influence on the performance of the stack during co-electrolysis mode. Recorded EIS data of the middle cell of the stack were fitted with an equivalent circuit model (ECM) consisting of an inductive unit, a serial resistor and three RQ elements connected in series. Figure 11 shows a comparison of EIS spectra at 1.4 (a) and 8 bar (b) with five different gas compositions. Pure steam electrolysis with a 90/10 (H_2O/H_2) mixture, co-electrolysis compositions with 60/30/10 and 45/45/10 ($H_2O/CO_2/H_2$) and CO_2-electrolysis with 90/10 (CO_2/H_2 and CO_2/CO) are investigated. For the co-electrolysis and the CO_2/H_2 compositions rWGS reaction can occur, whereas for the CO_2/CO mixture pure electrochemical reduction of CO_2 is ensured. The measurements were recorded at a stack temperature of 780 °C and a current density of −0.2 A·cm^{-2}. The outlet gas composition of the stack was close to a 60/40 reactant/product mixture where the concentration impedance is highly reduced due to the more balanced composition between reactants and products in the cells.[28] Due to the different inlet gas compositions, the furnace temperature had to be adjusted in order to ensure an equal stack temperature and thus similar serial resistances for all recorded measurements.

The comparison between the EIS spectra recorded at 1.4 and 8 bar shows an apparent influence of the operating pressure. The peak in the –Z″(f) diagram for the process at 0.1–0.5 Hz becomes less prominent and shows a decreased frequency at elevated pressure. The resistance in this range of frequency can be attributed to gas concentration, the coupled phenomena of diffusion and reactant conversion taking place within the fuel electrode compartment.[28–32] The conversion impedance itself occurs due to the deviation between the supplied reactant concentrations and the actual gas concentrations at the electrode surface during operation. This resistance becomes generally more significant with an increasing imbalance between H_2O/H_2 or CO_2/CO. Considering the SOC to behave as a continuous stirred tank reactor (CSTR), the resistance of the conversion impedance R_{conv} is pressure independent whereas the capacitance C_{Conv} increases linearly with increasing pressure.[30,33]

$$R_{conv} = \frac{RT}{4F^2 J_i}\left(\frac{1}{x_{i,\,educt} + x_{i,\,product}}\right)$$

$$C_{conv} = \frac{4F^2 pV}{(RT)^2 A}\left(\frac{1}{x_{i,\,reactant} + x_{i,\,product}}\right)^{-1}$$

where J_i is the area specific inlet gas flux with the unit of mol cm^{-2} s^{-1}, $x_{i,reactant}$ and $x_{i,product}$ are the specific mole fractions in the inlet gas. *p* is the absolute pressure, *V* the CSTR volume and *A* the geometric electrode area. Primdahl et al. showed that the conversion capacitance increases with increasing pressure, since the volumetric density of reactants and products within the fuel electrode compartment increase.[31,33] Consequently, the frequency *f* of the conversion process decreases at elevated pressure and follows a p^{-1} dependency due to the relation $f = 1/(2\pi \cdot R \cdot C)$. Due to keeping constant the relevant parameters (flux of gases, stack temperature, 90/10 mixture as inlet composition, current density) for all EIS measurements one can assume the R_{conv} to be equal for all experiments shown in Fig. 11 and only the capacitance C_{Conv} to change due to the operating pressure. As the diffusion of CO_2 compared to H_2O (or CO compared to H_2) through a porous layer or a gas layer is generally more hindered due to its larger molecule size and molecular mass, the change in the observed peak at 0.1–0.5 Hz can most likely be

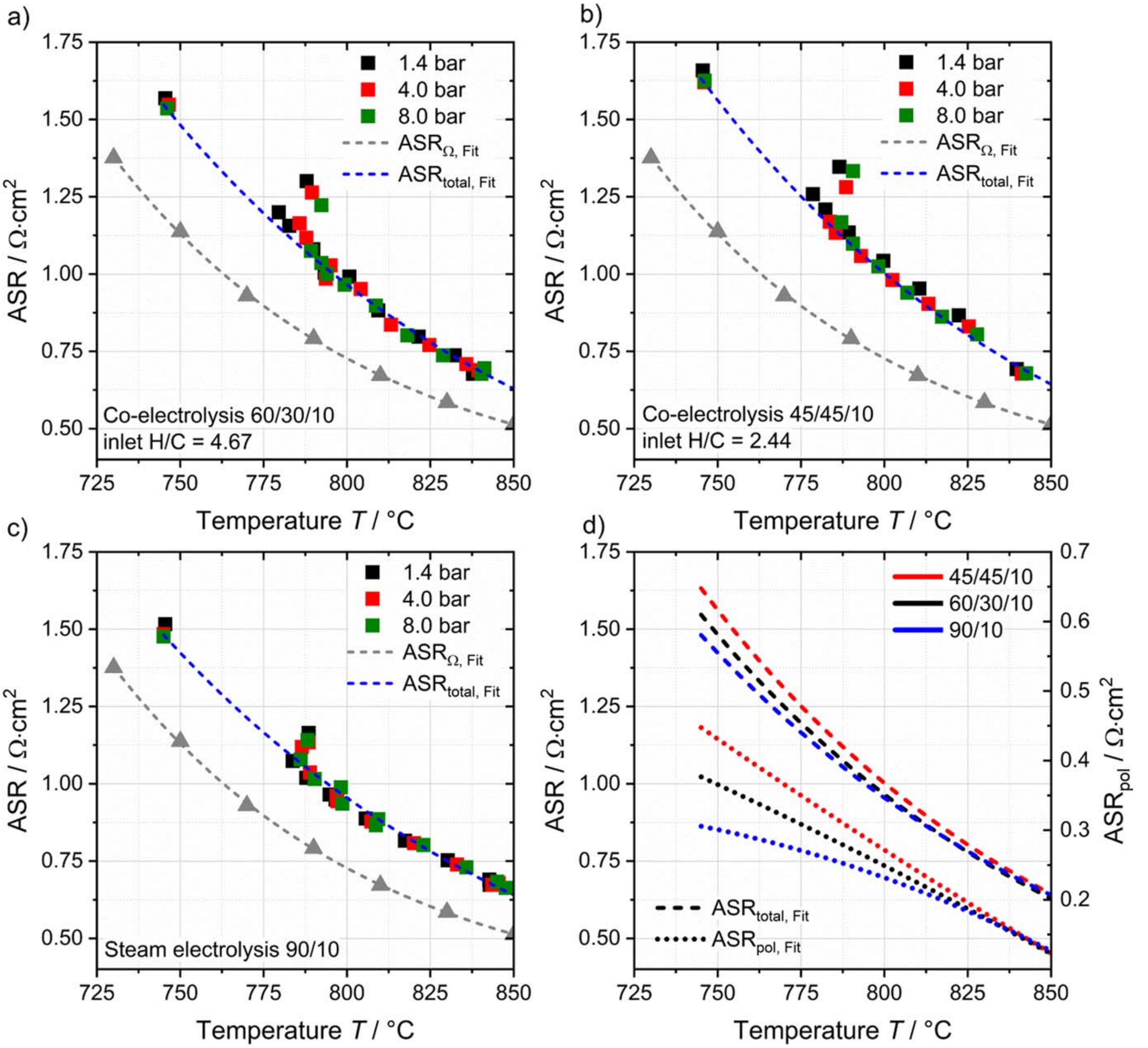

Figure 10. ASR values derived from U(i) characteristics for co-electrolysis (a), (b) and pure steam-electrolysis (c). (d) shows the fitted *ASR* curves of a-c. Values of the temperature-dependency of the ohmic resistance derived from.[18]

attributed to a diffusion process within the fuel electrode compartment. The diffusion resistance R_{Diff} has the following expression:

$$R_{Diff} = \left(\frac{RT}{2F}\right)^2 \frac{l}{pD_{eff}} \left(\frac{1}{x_{b,educt}} + \frac{1}{x_{b,\ product}}\right)$$

with x_b as the mole fraction of reactant and product in the bulk gas outside the diffusion layer or porous electrode and D_{eff} as the effective diffusion coefficient consisting of the Knudsen (D_K) and ordinary diffusion coefficients (D_{ord}). At low pressure, diffusion is governed by Knudsen diffusion mechanism. Knudsen diffusion itself is pressure independent and the diffusive mass flux is therefore governed by the concentration gradient which is directly proportional to pressure. At higher pressure, diffusion becomes governed by ordinary diffusion mechanism which is reciprocally proportional to pressure. Hence, the effective diffusion coefficient D_{eff} decreases nonlinearly with increasing pressure. However, the slight decrease of D_{eff} nevertheless leads to an increase of the term $p{\cdot}D_{eff}$ by increasing the pressure. A detailed theoretical study about the operating pressure dependency of D_{eff} for SOCs can be found elsewhere.[22,34] In conclusion, R_{Diff} decreases with increasing pressure according to the above mentioned equation. The lower resistance at elevated pressure consequently leads to a decreased height of the peak around 0.5 Hz in the –Z'(f) diagram of Fig. 11. Jensen et al. conducted stack measurements at elevated pressure and showed that the low frequency peak shifts towards lower frequencies by increasing the operating pressure.[10] This is in good agreement with the EIS measurement shown in Fig. 11 for steam, co- and CO_2 electrolysis where the same phenomenon was observed. However, a decreased resistance of the low frequency process was not observed within the study of Jensen et al. This is most likely due to the fact that the measurements were conducted at *OCV*, whereas the measurements shown in Fig. 11 were conducted under significant load. The increased extent of reaction leads to a significantly more dominant diffusion of reactants and products and hence to a more dominant pressure effect.

Figure 11 reveals the process-related peak and the resistance at a frequency of 10–20 Hz to become less prominent with higher

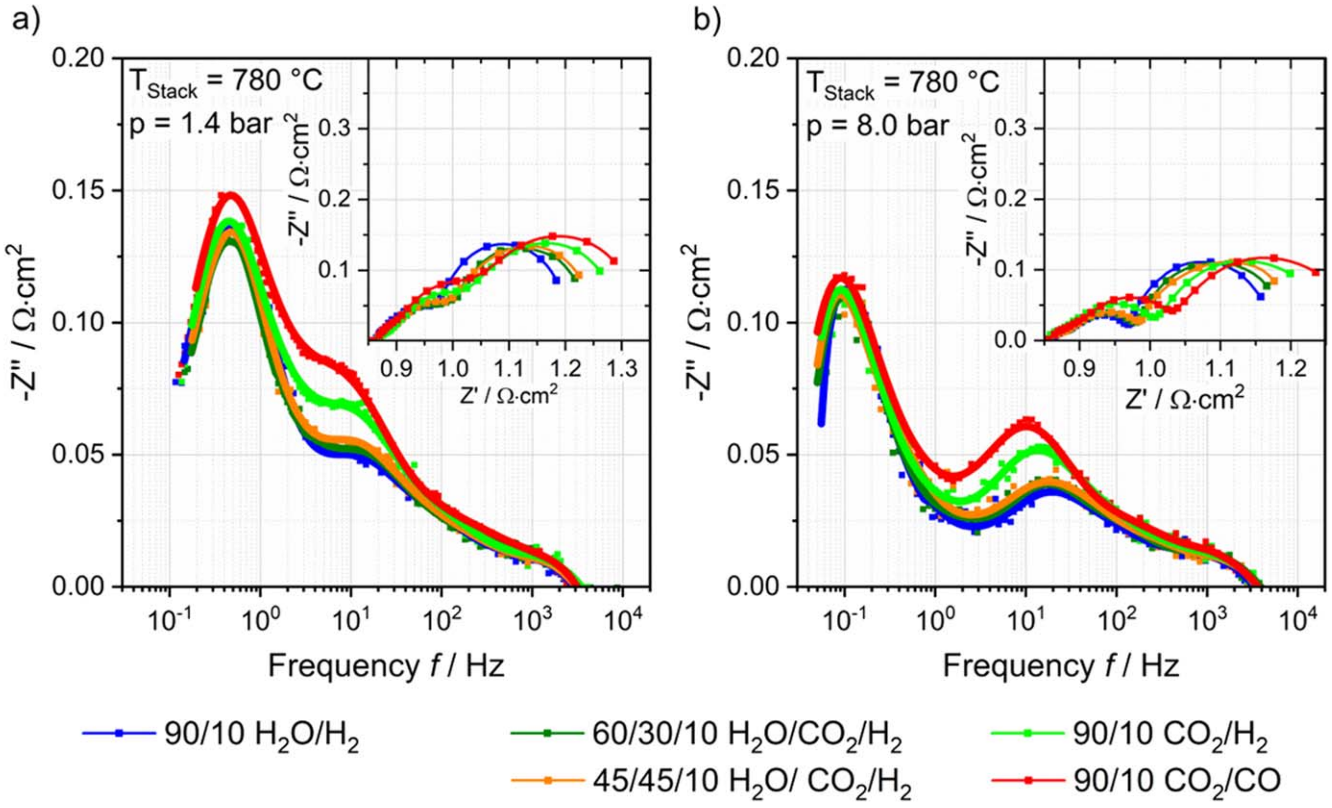

Figure 11. Comparison of five gas compositions for steam, co- and CO_2-electrolysis at 1.4 (a) and 8 bar (b). A reactant conversion of 30% and a current density of −0.20 A·cm^{-2} was chosen for the EIS spectra.

operating pressure. Since this middle frequency process shows a dependency on the partial pressures of the reactants, it can likely be attributed to a surface process at the fuel electrode. With higher pressure the resistance decreases due to the increased concentration of reactants at active sites and the frequency in the EIS spectrum therefore decreases. Additionally the peak and the resistance can be observed to get more prominent with an increasing content of CO_2 in the feed gas for 1.4 and 8 bar respectively. This can be attributed to the decreasing partial pressure of H_2O within the porous electrode and a related increase of the activation resistance. Albeit the activation energy of electrochemical CO_2 reduction is reported to be higher than that for steam reduction, it is nonetheless likely that CO_2 is reduced electrochemically to some extent especially at high conversion rates.[27,35] Since a low partial pressure of H_2 reduces the rate of the rWGS reaction, it can be assumed that the electrode potential increases locally at the beginning of the cell area due to the increased diffusion and activation resistance of the CO_2 process. With increased cell length, the CO production pathway is then shifted towards the rWGS reaction due to the increased partial pressure of produced H_2. Since the recorded EIS measurements shown in Fig. 11 constitute an average of the SOC performance due to the large cell area of the used stack, the difference between pure steam- and co-electrolysis gas compositions is found to be marginal. Hence, it can be assumed that the main reaction pathway for the production of CO during co-electrolysis operation is via the fast rWGS reaction.[16,36]

Since the influence of CO_2 in the feed gas on the characteristic performance of the stack was shown to be most dominant at low temperatures, a direct comparison between pure steam and pure CO_2 electrolysis is shown in Fig. 12 for 700 °C and 850 °C. In addition to the EIS spectra plotted in a –Z″(f) diagram, the values for the ASR_{total} and the middle and low frequency resistances (R_{MF} and R_{LF}) are given in Table II according to the ECM with one inductive unit, a serial resistor and three RQ elements connected in series. The high frequency process (10^2–10^3 Hz) was not analyzed in detail since it is most likely attributable to the air electrode and should not differ between H_2O and CO_2 electrolysis due to the same RC.[37] However, several studies show that the contribution of a CGO bulk process of the fuel electrode is most likely located additionally within the high frequency range.[38,39] Hence, the high frequency process cannot be assigned to one single process though the data was fitted with a single RQ element and a constant n-value of 0.5. The authors are aware that the n-value of 0.5 for the high frequency process(es) do physically not make sense and indicate that a Gerischer element could be used for a more physically meaningful fit of the air electrode. However, due to the mentioned overlap (air electrode + CGO bulk) the authors decided to use a single RQ element to reduce the number of fitting parameters. Furthermore, the purpose of this study was to describe the changes in the impedance spectra during H_2O and CO_2 electrolysis for the middle and low frequency processes. The n-values during the fitting procedure were kept constant for all RQ elements according to Table II. Note that the raw data and the fitted spectra are plotted jointly in Fig. 12.

At 700 °C the difference between steam and CO_2 electrolysis is observed to be significant for the middle and low frequency processes attributed to the fuel electrode and the concentration impedance respectively. At 1.4 bar the gas concentration resistance shows significantly higher values during CO_2 electrolysis compared to pure steam electrolysis operation (see Table II). Since the resistance of the gas conversion is considered to be equal due to the same amount of reactant moles and volume flows in both cases, the difference can be attributed to a more signifcant diffusion resistance for CO_2 electrolysis operation. However, both operation modes show similar frequencies for the respective low frequency peak which indicates a significant change of the capacitance for the CO_2/CO operation. At higher pressure (Fig. 12b) the diffusion resistance decreases due to superior mass transport and the peaks are shifted towards lower resistance values and lower frequencies. The middle frequency peak attributed to the fuel electrode process shows higher values for CO_2 electrolysis and consequently a decreased

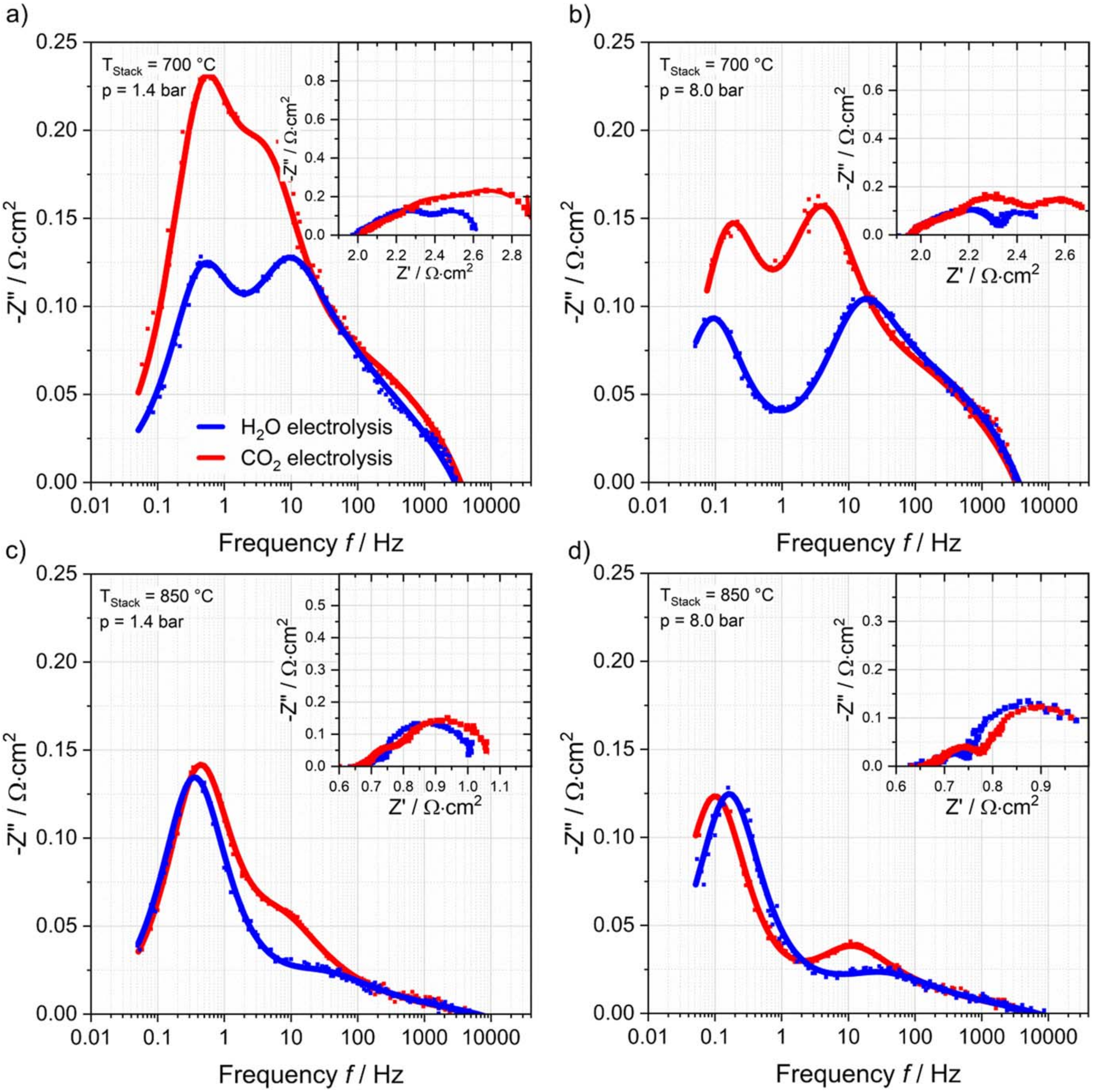

Figure 12. Comparison of EIS spectra during steam and CO_2 electrolysis operation at 700 °C and 850 °C respectively and 1.4 and 8 bar of pressure. *RC* is 30% at a current density of $-0.20\ \mathrm{A \cdot cm^{-2}}$.

frequency compared to pure steam electrolysis operation. The decrease of the resistance at elevated pressure is observed to be more significant for the CO_2 electrolysis indicating a significantly higher pressure sensitivity compared to pure steam electrolysis.

At a stack temperature of 850 °C the middle frequency resistance at 1.4 and 8 bar show lower values due to the generally faster kinetics at higher temperature. The low frequency process is observed to be similar for steam and CO_2 electrolysis respectively, which could indicate an equal diffusion rate of the reactants through the porous layer. The middle frequency process shows slightly higher resistances for CO_2 reduction compared to steam reduction at both 1.4 and 8 bar. However, in relation to the ASR_{total}, the proportion of R_{MF} is marginal in both operation modes and at both pressures whereas the conversion and diffusion part takes almost a proportion of one fourth of the ASR_{total} at 850 °C in this study. Since the concentration impedance for steam and CO_2 electrolysis is found to be similar at high temperatures and the influence of the fuel electrode process on the ASR_{total} is marginal, it can be concluded that the overall performance of the ESC stack is similar in both operation modes at high operating temperature. Lower operating temperatures are observed to lead to a more significant influence of the low and middle frequency processes and thus to a more significant performance loss during CO_2 electrolysis operation. This observation is congruent with the findings for the ASR_{total} characteristics of the co-electrolysis operation shown in Fig. 10 where a correlation between a higher CO_2 content in the feed gas and an increased ASR_{total} was observed. However, the current theory based on the equations for R_{diff} and R_{conv} predict both the diffusion and conversion resistances to increase with higher temperatures. While this is in accordance with the impedance results of the low frequency part of the spectra

Table II. Values of the middle and low frequency resistances (R_{MF} and R_{LF}) and the total resistance (ASR_{total}) at the two operating temperatures and pressures according to the spectra shown in Fig. 12. N-values of the RQ elements were kept constant during the fitting procedure.

	H_2O electrolysis				CO_2 electrolysis			
	700 °C		850 °C		700 °C		850 °C	
Pressure	1.4 bar	8 bar	1.4 bar	8 bar	1.4 bar	8 bar	1.4 bar	8 bar
$R_{HF}/\Omega\cdot cm^2$	0.27	0.25	0.07	0.07	0.29	0.27	0.07	0.07
n value	0.50	0.50	0.50	0.50	0.50	0.50	0.50	0.50
$R_{MF}/\Omega\cdot cm^2$	0.18	0.16	0.02	0.02	0.29	0.28	0.07	0.06
n value	0.90	0.90	0.90	0.90	0.90	0.90	0.90	0.90
$R_{LF}/\Omega\cdot cm^2$	0.20	0.19	0.26	0.25	0.37	0.25	0.27	0.25
n value	0.99	0.99	0.99	0.99	0.99	0.99	0.99	0.99
ASR_{total}	2.61	2.55	1.02	0.99	2.93	2.74	1.07	1.03

recorded for steam electrolysis, it is not the case for pure CO_2 electrolysis. Furthermore one would expect the Knudsen diffusion to be more dominant at lower temperature due to the proportionality between the mean free path for the gas molecules and the operating temperature. As described above, Knudsen diffusion itself is pressure independent. Hence, one would expect a higher pressure dependency of the stack at higher operating temperatures. It could be speculated that an additional electrochemical process may be located within the low frequency part of the spectra which could explain the observed behavior. However, this could not be identified within the presented study. Hence, the described temperature behavior during CO_2 electrolysis and the related decrease of the low frequency resistance by increasing the temperature is currently not fully understood and need to be investigated in more detail for the used Ni-CGO electrodes.

Conclusions

Pressurized operation, high conversion rates during co-electrolysis and high partial pressures of CO in the outlet gas composition increase the risk of solid carbon formation in the outlet pipes of SOC test rigs. Since a clogging of the pipe would be related to a damage of the stack, an approach for the prevention of carbon deposition was introduced and could successfully be demonstrated for all measurements shown in this study. A commercially available 10 layer SOC stack was used for an experimental characterization in steam, co- and CO_2-electrolysis mode. The investigated stack consists of electrolyte supported cells with Ni/CGO fuel electrodes and LSCF air electrodes. Test results for steady-state and dynamic operation were demonstrated under elevated operating pressures up to 8 bar. Furthermore EIS analysis was performed in order to investigate the pressure dependency of the SOC performance during co- and CO_2-electrolysis in more detail.

Gas analysis at *OCV* condition with different inlet volume flows showed that the gas composition at the outlet of the stack was found to be generally in good accordance with the calculated thermodynamic equilibria. Firstly, this indicates the precise supply of the feed gases and the analytical system to work accurately over a wide range of operation in this study. Secondly, it shows that the chemical reactions are fast and the catalytic surface is sufficiently active and available to equilibrate the inlet gases rapidly within the cells via the reverse water-gas shift reaction (rWGS).

Steady-state measurements in co-electrolysis mode with inlet gas compositions with a H/C ratio of 4.67 (60/30/10 $H_2O/CO_2/H_2$) and 2.44 (45/45/10 $H_2O/CO_2/H_2$) were performed at 1.4, 4 and 8 bar with a conversion of 70%. The results show that the cell voltages increase at elevated pressure as predicted by the Nernst equation. With increasing current density, the cell voltages of the different pressure levels were found to converge due to decreased activation and diffusion resistances. However, the observed convergence was primarily due to the increased stack temperature which is related to the occurring exothermic methanation reaction during co-electrolysis operation. Since the polarization resistance of the electrolyte supported cells used in the studied stack are comparably low (pressure independent ohmic resistance ~70% of entire cell resistance), a positive pressure effect on the limiting current density could not be observed. The gas analysis showed a good correlation between experiment and the stack temperature-based calculated thermodynamic equilibrium in all measurements.

Dynamically recorded $U(i)$-curves were performed both in steam- and co-electrolysis mode. Due to the additionally occurring endothermic rWGS reaction in co-electrolysis, the stack is affected by a more significant cooling effect and shows a slightly lower performance compared to steam electrolysis. However, an estimation of the influence of the reduced temperature on the ohmic resistance indicated that the performance and the *ASR* within the studied conditions in pure steam- and in co-electrolysis are highly similar.

Out of the steady-state and dynamic measurements, *ASR* values were derived for both steam and co-electrolysis operation over a wide temperature range. It was clearly observed that the *ASR* increases with lower H/C ratios at lower temperatures whereas it shows similar values at temperatures above 820 °C. The observation of an increasing *ASR* with increasing CO_2 content could possibly be explained by a higher resistance caused by the occurance of direct CO_2 electrolysis during co-electrolysis operation. It could be shown that the CO_2 reduction process reveal a higher activation resistance especially at lower temperatures. Furthermore the diffusion resistance during CO_2 electrolysis was found to show a significantly higher temperature dependence compared to pure steam electrolysis. However, for the studied co-electrolysis operation the difference of the activation and diffusion resistances was found to be marginal indicating that the main reaction pathway for CO production is via the rWGS. Since pure CO_2 electrolysis showed a higher proportion of activation and diffusion resistances compared to the pressure independent ohmic resistance of the cell, the pressure sensitivity was found to be significantly increased for that type of SOC operation mode.

References

1. European Commission, *A clean planet for all - A European Strategic Long-Term Vision For a Prosperous, Modern, Competitive and Climate Neutral Economy COM(2018)773* (2018) 1–25 https://ec.europa.eu/transparency/regdoc/rep/1/2018/EN/COM-2018-773-F1-EN-MAIN-PART-1.PDF.
2. H. Ibrahim, A. Ilinca, and J. Perron, "Energy storage systems-Characteristics and comparisons." *Renew. Sustain. Energy Rev.*, **12**, 1221 (2008).
3. A. Evans, V. Strezov, and T. J. Evans, "Assessment of sustainability indicators for renewable energy technologies." *Renew. Sustain. Energy Rev.*, **13**, 1082 (2009).
4. P. J. Hall and E. J. Bain, "Energy-storage technologies and electricity generation." *Energy Policy*, **36**, 4352 (2008).
5. A. Sternberg and A. Bardow, "Power-to-What?-environmental assessment of energy storage systems." *Energy Environ. Sci.*, **8**, 389 (2015).
6. J. C. Koj, C. Wulf, and P. Zapp, "Environmental impacts of power-to-X systems - A review of technological and methodological choices in life cycle assessments." *Renew. Sustain. Energy Rev.*, **112**, p. 865-879 (2019).

7. J. B. Hansen, N. Christiansen, and J. U. Nielsen, "Production of sustainable fuels by means of solid oxide electrolysis." *ECS Trans.*, **35**, 2941-2948 (2011).
8. G. A. Mills, "Status and future opportunities for conversion of synthesis gas to liquid fuels." *Fuel*, **73**, 1243 (1994).
9. X. Sun, M. Chen, S. H. Jensen, S. D. Ebbesen, C. Graves, and M. Mogensen, "Thermodynamic analysis of synthetic hydrocarbon fuel production in pressurized solid oxide electrolysis cells." *Int. J. Hydrogen Energy*, **37**, 17101 (2012).
10. S. H. Jensen, C. Graves, M. Chen, J. B. Hansen, and X. Sun, "Characterization of a planar solid oxide cell stack operated at elevated pressure." *J. Electrochem. Soc.*, **163**, F1596 (2016).
11. S. H. Jensen, X. Sun, S. D. Ebbesen, R. Knibbe, and M. Mogensen, "Hydrogen and synthetic fuel production using pressurized solid oxide electrolysis cells." *Int. J. Hydrogen Energy*, **35**, 9544 (2010).
12. J. E. O. Brien, X. Zhang, and G. K. Housley, *High Temperature Electrolysis Pressurized Experiment Design, Operation, and Results INL/EXT-12-26891* (2012) 1–15 https://inldigitallibrary.inl.gov/sites/sti/sti/5516323.pdf.
13. X. Sun et al., "Performance characterization of solid oxide cells under high pressure." *Fuel Cells*, **15**, 697 (2015).
14. E. C. Thomsen, G. W. Coffey, L. R. Pederson, and O. A. Marina, "Performance of lanthanum strontium manganite electrodes at high pressure." *J. Power Sources*, **191**, 217 (2009).
15. G. A. Hughes, J. Railsback, D. M. Butts, and S. A. Barnett, "Electrochemical performance of solid oxide cell oxygen electrodes under pressurization." *ECS Trans.*, **68**, 687 (2015).
16. S. D. Ebbesen, R. Knibbe, and M. Mogensen, "Co-electrolysis of steam and carbon dioxide in solid oxide cells." *J. Electrochem. Soc.*, **159**, F482 (2012).
17. C. Stoots, J. O'Brien, and J. Hartvigsen, "Results of recent high temperature coelectrolysis studies at the Idaho National Laboratory." *Int. J. Hydrogen Energy*, **34**, 4208 (2009).
18. M. Riedel, M. P. Heddrich, and K. A. Friedrich, "Analysis of pressurized operation of 10 layer solid oxide electrolysis stacks." *Int. J. Hydrogen Energy*, **44**, 4570 (2019).
19. B. J. Mcbride, M. J. Zehe, and S. Gordon, *NASA Glenn Coefficients for Calculating Thermodynamic Properties of Individual Species NASA/TP-2002-211556* (2002) 1–283https://www.grc.nasa.gov/WWW/CEAWeb/TP-2002-211556.pdf.
20. S. Santhanam, M. P. Heddrich, M. Riedel, and K. A. Friedrich, "Theoretical and experimental study of reversible solid oxide cell (r-SOC) systems for energy storage." *Energy*, **141** (2017).
21. M. Henke, J. Kallo, K. A. Friedrich, and W. G. Bessler, "Influence of pressurisation on SOFC performance and durability: A theoretical study." *Fuel Cells*, **11**, 581 (2011).
22. M. Henke, C. Willich, J. Kallo, and K. A. Friedrich, "Theoretical study on pressurized operation of solid oxide electrolysis cells." *Int. J. Hydrogen Energy*, **39**, 12434 (2014).
23. L. Bernadet, G. Gousseau, A. Chatroux, J. Laurencin, F. Mauvy, and M. Reytier, "Assessment of pressure effects on high temperature steam electrolysis based on solid oxide technology." *ECS Trans.*, **68**, 3369 (2015).
24. M. Henke et al., "A validated multi-scale model of a SOFC stack at elevated pressure." *Fuel Cells*, **13**, 773 (2013).
25. S. D. Ebbesen, X. Sun, and M. B. Mogensen, "Understanding the processes governing performance and durability of solid oxide electrolysis cells." *Faraday Discuss.*, **182**, 393 (2015).
26. X. Yue and J. T. S. Irvine, "Alternative cathode material for CO_2 Reduction by high temperature solid oxide electrolysis cells." *J. Electrochem. Soc.*, **159**, F442 (2012).
27. V. Menon, Q. Fu, V. M. Janardhanan, and O. Deutschmann, "A model-based understanding of solid-oxide electrolysis cells (SOECs) for syngas production by H_2O/CO_2 co-electrolysis." *J. Power Sources*, **274**, 768 (2015).
28. W. G. Bessler and S. Gewies, "Gas concentration impedance of solid oxide fuel cell anodes." *J. Electrochem. Soc.*, **154**, 548 (2007).
29. T. Jacobsen, P. V. Hendriksen, and S. Koch, "Diffusion and conversion impedance in solid oxide fuel cells." *Electrochim. Acta*, **53**, 7500 (2008).
30. M. B. Mogensen, S. D. Ebbesen, S. H. Jensen, X. Sun, A. Hauch, and M. Chen, "Concentration impedance in testing of solid oxide cells revisited." *ECS Trans.*, **78**, 2133 (2017).
31. S. Primdahl, "Gas conversion impedance: a test geometry effect in characterization of solid oxide fuel cell anodes." *J. Electrochem. Soc.*, **145**, 2431 (1998).
32. Y. Tanaka, M. P. Hoerlein, and G. Schiller, "Numerical simulation of steam electrolysis with a solid oxide cell for proper evaluation of cell performances." *Int. J. Hydrogen Energy*, **41**, 752 (2016).
33. S. Primdahl, "Gas diffusion impedance in characterization of solid oxide fuel cell anodes." *J. Electrochem. Soc.*, **146**, 2827 (1999).
34. M. Henke, J. Kallo, K. A. Friedrich, and W. G. Bessler, "Influence of pressurisation on SOFC performance and durability: a theoretical study." *Fuel Cells*, **11**, 581 (2011).
35. J. Aicart, M. Petitjean, J. Laurencin, L. Tallobre, and L. Dessemond, "Accurate predictions of H_2O and CO_2 co-electrolysis outlet compositions in operation." *Int. J. Hydrogen Energy*, **40**, 3134 (2015).
36. J. Wei and E. Iglesia, "Isotopic and kinetic assessment of the mechanism of reactions of CH_4 with CO_2 or H_2O to form synthesis gas and carbon on nickel catalysts." *J. Catal.*, **224**, 370 (2004).
37. Q. Fang, C. E. Frey, N. H. Menzler, and L. Blum, "Electrochemical performance and preliminary post-mortem analysis of a solid oxide cell stack with 20,000 h of operation." *J. Electrochem. Soc.*, **165**, F38 (2018).
38. S. Primdahl and M. Mogensen, "Mixed conductor anodes: Ni as electrocatalyst for hydrogen conversion." *Solid State Ionics*, **152–153**, 597 (2002).
39. M. Riegraf, R. Costa, G. Schiller, K. A. Friedrich, S. Dierickx, and A. Weber, "Electrochemical impedance analysis of symmetrical Ni/gadolinium-doped ceria (CGO10) electrodes in electrolyte-supported solid oxide cells." *J. Electrochem. Soc.*, **166**, F865 (2019).